A Study on the Performance of Liquid Adhesive in Sealing a Split Magnetic Device

Huitao Zhang [1,2,a], Decai Li[1,b*]

[1] *School of Mechanical, Electronic and Control Engineering, Beijing Jiaotong University, Beijing* 100044 *China*
[2]*School of computer science, Shijiazhuang University, Shijiazhuang* 050035 *China*
[a]12116317@bjtu.edu.cn , [b]decli@bjtu.edu.cn

***Abstract* — A split magnetic liquid sealing combines the magnetic liquid rotary sealing and the adhesive plane sealing. Based on the Volkersen shear-lag model theory, this paper utilizes the finite element method to analyze the glue coating under the influence of normal and tangential joint loading. Also, we analyze the influence of the size and interface topography of different surfaces on the sealing performance. The results indicate that with increasing roughness, i.e. increasing micro-pit depth, the stress of Mises on the wave crest reduces and the stress of Mises on the wave hollow increases. The closer to the interface, the more obvious the effects are, and the maximum is located between the interfaces. Under the same roughness, the sealing performance is the best when the interface topography is the sinusoid and the sealing performance is the worst when the interface topography is the curved generatrix because the surface curvature increases clearly and the stress concentration is easier to occur. The simulated results can provide reference for the sealing performance evaluation of different sealing devices and the estimation of the critical stress at the time of interface failure.**

Keywords - split magnetic liquid sealing; interface size; interface topography; stress; sealing performance.

I. INTRODUCTION

As a new functional material, magnetic fluid not only has the fluidity but also the magnetism of solid material. Under the effect of magnetic field, the magnetic fluid presents many features which are not owned by the normal liquid. [1-5].Magnetic fluid sealing technology uses the changes of high saturation magnetic fluid in response to the magnetic field to seal the related equipment.[6-10]The split magnetic liquid sealing technique is a new technique for the replacement, maintenance, commissioning, research and development of the sealing elements of the large-scale mechanical equipment. When the electric machine breaks down, it only needs to disassemble the sealing elements of the whole equipment, and thus saving a lot of the manpower and material resources. It not only has the advantages of zero leakage of the magnetic liquid, long service life, high dependability, no pollution, self-recover ability, and ability to bear the high rotation speed, small change of torque, simple structure, and easy production [11-16] but also solves the complex issue of disassembly and installation for inspection and maintenance with high practical value and economic value.

The design of sealing technique of the adhesive surface is a key technique of the split magnetic liquid sealing. It focuses on the adhesive technique of the external half shells. The effects of the adhesive have direct impact on the result of sealing. The microscopic concave and convex interface topography of the adhesive surface not only influences the adhesive strength and stress distribution, but also leads to the disbanding coating and slabbing, and even sealing failure. Therefore, it is vital to study the size and the topography of the microscopic interface.

Currently, the sealing techniques of the magnetic liquid receives much attention and develops rapidly. Li Decai deduced the equation of anti-pressure of the magnetic liquid [17]. Yang Xiaolong and Li Decai utilized the finite element numerical method to calculate the magnetic field in the magnetic liquid sealing structure so that they calculated the anti-pressure ability of the magnetic liquid [18]. However, because that the magnetic liquid sealing structure is integrated with the axle, it is difficult to conduct replacement, maintenance, and commissioning. In 2007, Boyson proposed the reliability problem of applying the split sealing techniques [19]. Saito C, Belli S , et al. applied the technology of adhesive sealing to the medical field [20-21]. Based on this, the paper combines the magnetic liquid sealing techniques and the adhesive sealing techniques and gets a split magnetic liquid sealing structure. This paper analyzes and studies the influence of different interface's size and topography on the stress with the change of temperature through finite element analysis for the matrix layer, adhesive layer, and plane strain model. In the end, this paper gets the influence on the split magnetic liquid sealing performance.

II. THE THEORETICAL ANALYSIS OF THE PLANE SEALING PERFORMANCE OF THE SPLIT MAGNETIC LIQUID ADHESIVE [22-23]

A. The plane sealing structure of the split magnetic liquid adhesive

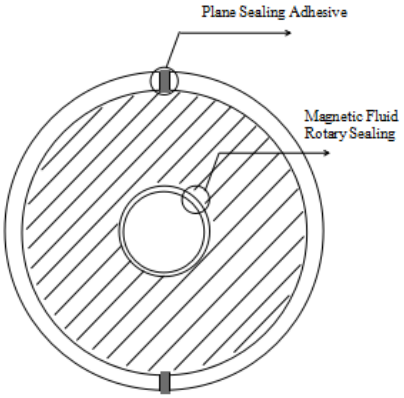

Fig 1 The radial section at the pole shoe of the split magnetic liquid sealing structure

Figure 1 is the radial section at the pole shoe of the split magnetic liquid sealing structure. The cylinder in the middle is the axle, the shadow is the pole shoe, and the space between them is sealed by the magnetic liquid. The outermost are the two half shells, the adhesive plane of the shell is plane and is sealed by the glue. There it is clear that the split magnetic liquid sealing is the combination of the magnetic liquid rotary sealing and adhesive plane sealing.

B. The theoretical calculation of the sealing performance of the split magnetic liquid adhesive plane

Supposing that the adhesive only has shear deformation under the influence of the radial pressure and loading, the connected only has tensile deformation and the thickness direction of the adhesive's shearing strength remains the same. Supposing that the adhesive layer is only influenced by the shear stress and strain and the elastic stress and material between the adhesive line and adhesive material are isotropic. Supposing that the bending moment caused by the non-coaxiality is ignored. Supposing that the ignoring the loading caused rotation of the adhesive and resulted the nonlinear effects of the adhesive layer. Based on the above suppositions, the second-order equation deduced from the Volkersen shear-lag model theory is shown as follows:

$$\tau'' - \omega^2 \tau = 0 \tag{1}$$

$$\omega^2 = \left(\frac{Gb}{d}\right)\left[\frac{1}{A_1 E_1} + \frac{1}{A_2 E_2}\right] \tag{2}$$

G is the shear modulus of the adhesive layer, d is the thickness, b is the width, A_1E_1 and A_2E_2 is the axial rigidity of the upper and lower adhesive. The shear strength of the adhesive is:

$$\tau = C_1 \cosh(\omega x) + C_2 \sinh(\omega x) \tag{3}$$

The constants C_1 and C_2 are decided by the boundary load.

$$\tau_{\max} = \frac{PG}{d\omega}\left(\frac{1}{E_1 A_1 \tanh(\omega L)} + \frac{1}{E_2 A_2 \sinh(\omega L)}\right) \tag{4}$$

III. THE ESTABLISHMENT OF THE FINITE ELEMENT MODEL

Supposing that the glue coating and the base are good bonding with each other, the upper and lower half shells are symmetrical(as is shown in figure 2), and establish the model of matrix, glue coating, and matrix. Because the thickness of the matrix is far greater than that of the glue coating, and the matrix is made of the 304 stainless steel rigid material, suppose it will nor deform so it will not have any influence on the simulation result to have the matrix thickness of 1mm. The glue coating uses the TONSAN 1596 silicone rubber with the thickness of 1mm. The characteristics of the matrix and the glue coating's material are shown in the table1. All the displacement of the nodes on the upper and lower line of the model has fixed constraints. To have higher accuracy when calculating the stress, refine the grind near the contact zone. The element type applied is CPE4T. There are 1,865 nodes in total (as shown in figure3

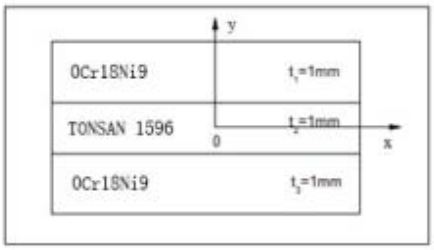

Fig.2 Schematic diagram of the model of matrix and glue coating and matrix

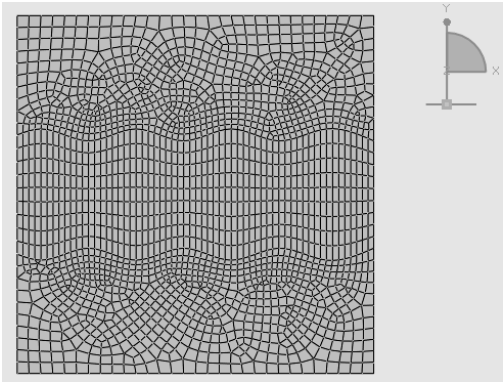

Fig.3 Finite element mesh of the model.

Use the sine curve to study the influence of the interface size on the residual stress under the temperature

change so get the influence on the split magnetic liquid sealing performance. The interface size of the sine curve refers to the change of the micro-pit depth.

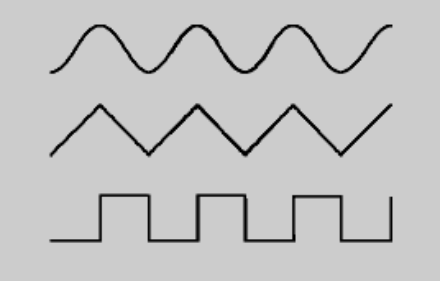

Fig.4 Microscopic interface model of different interface morphology.

The different microcosmic interface topographies are shown in figure4 to study the influence of different interface topography on the split magnetic liquid sealing performance. Suppose the glue coating and the upper and lower matrixes are ideally thermal contacted with each other, in other words, the temperature and the thermal current is continuous. The temperature caused by the rotation of the internal axis or the external heat source increases and then removes the heat source to reduce the temperature to the room temperature, 25°C so that the glue coating is influenced by the temperature difference. This paper defines the temperature difference is 25°C. Supposing that various material parameters are definite and the parameter reference of the material surface in the glue coating [24] is shown in the table 1 within that temperature range. This paper studies on the influence of the interface size and topography on the residual stress under the temperature change so as to have the influence on the split magnetic liquid sealing performance.

TABLE.1 THE MATERIAL PARAMETERS OF MATRIX AND GLUE COATING

Material	Density （tonne/mm^3）	Elastic Modulus （MP）	Poisson's Ration	Coefficient of Thermal Expansion 10^{-6}/°C	Heat Capacity J/（g·°C）	Thermal Conductivity W/（mm·°C）
TONSAN 1596	0.97×10^{-9}	2	0.49	310	1.46	0.00015
304 Stainless Steel	7.93×10^{-9}	205000	0.3	17.3	0.5	0.0162

IV. RESULTS AND ANALYSIS

A. The total stress analysis and the interface size and topography

The main judging standard on influencing the split magnetic liquid sealing performance are the max shear stress on the interface τ_{xy} and the max pressure stress σ_y, which are the τ_{xy} and σ_y in the direction of *xy*[25]. Besides, according to that the elastic-plastic theory needs to consider the influence of the equivalent stress of Mises, the Mises pressure should be :

$$\sigma' = \{\frac{1}{2}[(\sigma_1 - \sigma_2)^2 + (\sigma_2 - \sigma_3)^2 + (\sigma_3 - \sigma_1)^2]\}^{1/2} \geq S_y \tag{5}$$

In the equation (5), σ' is the equivalent stress of Mises, σ_1, σ_2 and σ_3 are the first, second, and third principal stress and S_y is the local yield strength. In the following, this paper will focus on explaining the distribution conditions of the different simulative shear stress and pressure stress and the equivalent stress of Mises of the micro-pit depth and interface topography.

The interface size utilizes the following function to simulate. The micro-pit depth *h* is the amplitude and is represented by *A*; the micro-pit width λ is wave length and it is determined by the sinusoid curve:

$$y = A\sin\left(\frac{2\pi}{\lambda}x\right) \tag{6}$$

Because the roughness of the interface R_a and *A* are in a direct proportion, which is to say: $\frac{A}{R_a} = \frac{\pi}{2} = 1.55$ [26], so the change of the roughness can be simulated through changing the amplitude *A*. Because the roughness of the adhesive surface of the split magnetic liquid sealing equipment **Error! Reference source not found.**μm, A∈ [2.48, 80. 6] μm. This paper's model chooses A to be 80, 50, and 20μm to simulate the distribution conditions of the corresponding stress.

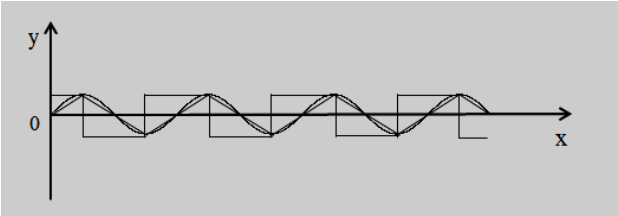

Fig. 5 Sketch map of different interface morphology.

Figure 5 is the sketch map of different interface morphology. The microscopic interface topography of the sinusoid curve is indicated by equation (6). The broken line microscopic interface topography is simulated with the following functional equation:

Error! Reference source not found.

(7)

Concave and convex line microscopic interface topography is stimulated with the following functional equation:

$$\begin{cases} y = A & x\in[(n-\frac{5}{4})\lambda,(n-\frac{3}{4})\lambda] \\ x = \left(n-\frac{1}{2}\right)\frac{\lambda}{2} & y\in[-A,A] \\ y = -A & x\in[(n-\frac{3}{4})\lambda,(n-\frac{1}{4})\lambda] \\ & n\in[1,2,3\cdots] \end{cases}$$

Error! Reference source not found.

(8)

Simulate the corresponding stress distribution conditions for the above three curves' functional equation with the same roughness A=50 μm.

B. The influence of the interface size on the sealing performance

When the micro-pit depth h changes, the stress distribution on the matrix and adhesive interface are shown in the figure 6 to figure 8. The greater stress, the weaker sealing performance is

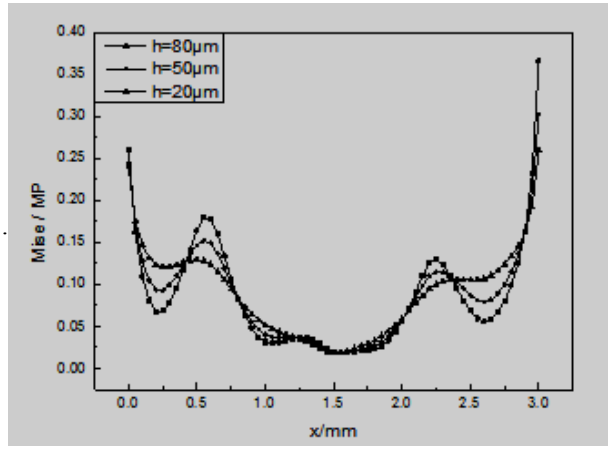

Fig. 6 The distribution along x-axle of the Mises stress with different micro pit depth.

Figure 6 is the distribution along x-axle of the Mises stress with different micro-pit depth. The depth of 0.2mm is the peak and wave crest and the depth of 0.6mm is the bottom and wave valley and so on with the wave length of 0.8mm. From figure 6, it is clear that in the wave crest, the stress of Mises decreases with the increasing depth of the micro-pit. In the wave valley, the stress of Mises increases with the increasing depth of the micro-pit and the closer to the boundary, the more obvious it is. The greatest stress of Mises is located in the two boundaries. The stress of Mises is greatest when the micro-pit depth of the outside boundary is 80 μm.

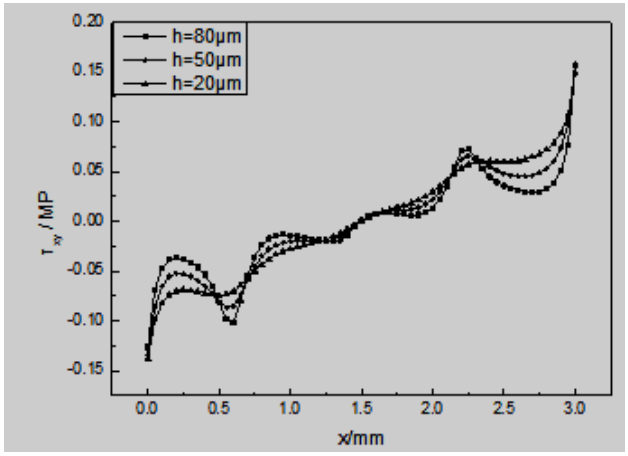

Fig.7 The distribution along x-axle of the shear stress τ_{xy} with different micro pit depth.

Figure 7 is the distribution along x-axle of the shear stress τ_{xy} with different micro pit depth. From figure 7, it is clear that the shear stress has two directions. The max shear stress is located in the two boundaries with the direction to the axis. When it is located in the wave crest, the shear stress τ_{xy} increases with the increasing

micro-pit depth. When it is locate in the wave valley, τ_{xy} decreases with the increasing micro-pit depth. The closer to the boundary, the more obvious the effects are.

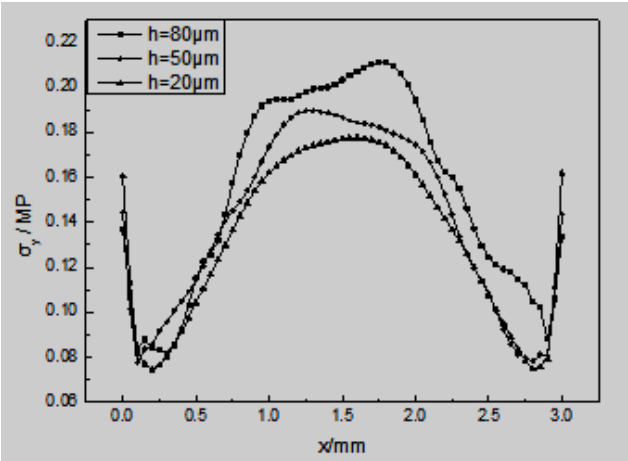

Fig.8 The distribution along x-axle of σ_y of y-axis with different micro pit depth.

Figure 8 is the distribution along x-axle of σ_y of y-axis with different micro pit depth. From figure 8, it is clear that when the temperature decreases, the σ_y of the y direction is the tensile stress. The greatest σ_y is located in the boundary and is about in the first wave crest and the last wave crest, where the model whose micro-pit depth has the greatest σ_y greater than the other two models. The σ_y stress near the boundary decreases with the increasing micro-pit depth.

C. The impact of micro-pit depth on the sealing performance

The micro-pit depth remains the same, which means the amplitude *A* remains the same. When the micro-pit depth changes, the stress distribution in the matrix and the adhesive coating is shown in figure 9 to figure 11. The greater the stress, the poorer sealing performance.

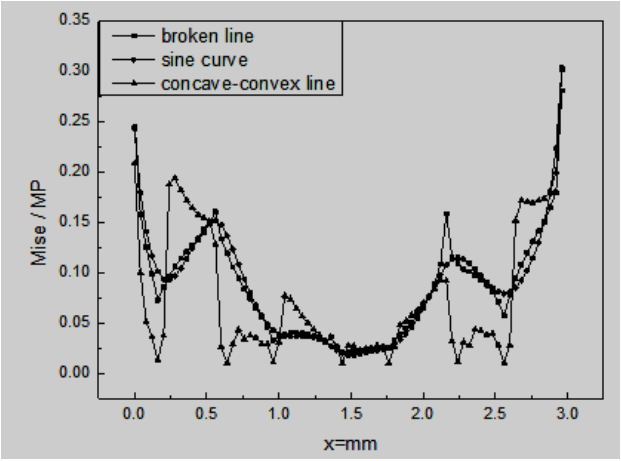

Fig. 9 The distribution along x-axle of the Mises stress with different micro pit morphology.

Figure 9 is the distribution along x-axle of the Mises stress with different micro pit morphology. From figure 9, it is clear that in the wave crest, the stress of Mises decreases with the increasing depth of the micro-pit. In the wave valley, the stress of Mises increases with the increasing depth of the micro-pit and the closer to the boundary, the more obvious it is. The max Mises stress is located in the boundaries.

As shown in figure 9, the stress curve of the broken line is similar with the stress curve of the sine wave. However, the stress concentration is more easily to occur when the stress curvature of the stress curve of the broken line increases obviously. The curvature of the concavo-convex line changes obviously, which means it is easy to have the many weak places of sealing leakage so it has the worst sealing performance.

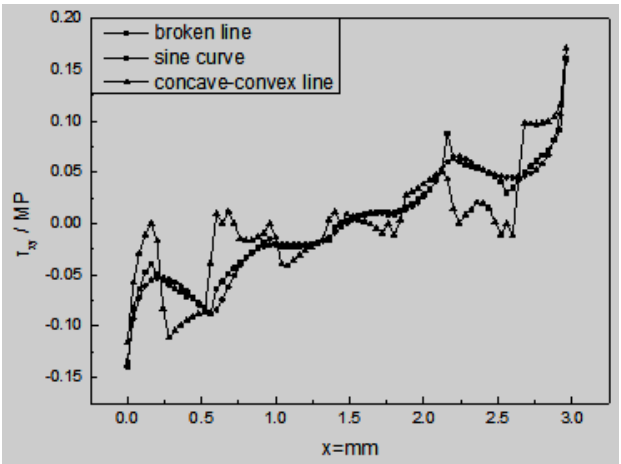

Fig.10 The distribution along x-axle of the shear stress τ_{xy} with different micro pit morphology.

Figure 10 is the distribution along x-axle of the shear stress τ_{xy} with different micro pit morphology. From

figure 10, it is clear that the shear stress has two directions. The max shear stress is located in the two boundaries with the direction to the axis. The max shear stresses τ_{xy} of three topography curve are located in the boundaries and are close to each other. However, from the analysis for the curvature change of the curve, the smallest influence of the sinusoid curve on the sealing performance, the more stable it is.

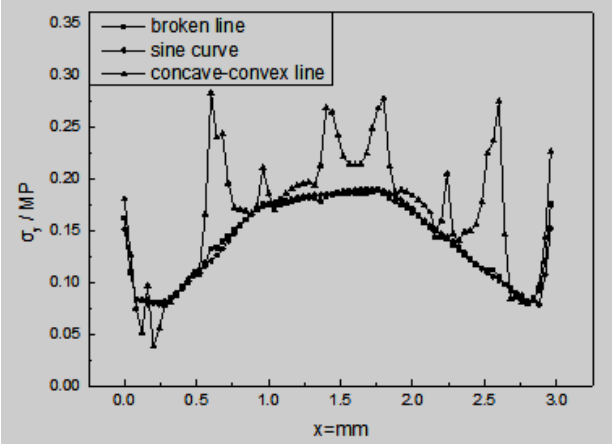

Fig.11 The distribution along x-axle of σ_y of y-axis with different micro pit morphology.

Figure 11 is the distribution along x-axle of σ_y of y-axis with different micro pit morphology. From figure 11, it is clear that when the temperature decreases, the σ_y of the y direction is the tensile stress. In view of that the curve and the σ_y stress curve of the sine are similar to each other. The greatest σ_y is located in the boundary and is about in the first wave crest and the last wave crest, where the model whose micro-pit depth has the greatest σ_y greater than the other two models. The curve values of the σ_y of the concavo-convex line is greater than the two other curves and has higher change frequency so it is easier to have stress concentration. Therefore figure 11 find out that utilizing the concavo-convex line microscopic interface is unfavorable for the enhancing sealing performance.

V. CONCLUSIONS

(1)This paper proposes the split sealing structure with combination of the magnetic liquid rotary sealing and adhesive plane sealing, and simulates the impact of the interface size and topography on the sealing performance of the sealing structure.

(2)With the increasing roughness, in other words, the increasing micro-pit depth, the stress of Mises on the wave crest reduces and the stress of Mises on the wave hollow increases. The closer to the interface, the more obvious effects are. The maximum is located at the both boundaries.

(3)Under the same roughness, the sealing performance is the best when the interface topography is the sinusoid, and the sealing performance is the worst when the interface topography is the curved generatrix because the curvature of the curve increases obviously and the stress concentration tends to occur.

(4)The result of simulation can provide reference for the base sealing performance evaluation of different sealing device and the estimation of the critical stress at the time of interface failure.

ACKNOWLEDGMENTS

This research was supported by the National Natural Science Foundation of China (Grant No. 51375039), Beijing Natural Science Foundation (Grant No. 4142046) and Program for Changjiang Scholars and Innovative Research Team (Grant No. IRT13046).

REFERENCES

[1] Guo C, Gong X, Xuan S, et al. Squeeze behavior of magnetorheological fluids under constant volume and uniform magnetic field[J]. Smart Materials & Structures, 2013, 22(4):361-373.

[2] Saga N, Nakamura T. Development of a peristaltic crawling robot using magnetic fluid on the basis of the locomotion mechanism of the earthworm[J]. Smart Materials & Structures, 2004, 13(13):566-569.

[3] Rosensweig R E. Ferrohydrodynamics [M]. New York: Dover Publications INC, 2002.

[4] Güth D, Schamoni M, Maas J. Magnetic fluid control for viscous loss reduction of high-speed MRF brakes and clutches with well-defined fail-safe behavior[J]. Smart Materials & Structures, 2013, volume 22(9):94010-94021(12).

[5] Upadhyay R V, Laherisheth Z, Shah K. Rheological properties of soft magnetic flake shaped iron particle based magnetorheological fluid in dynamic mode[J]. Smart Materials & Structures, 2014, 23(1):203-208.

[6] Kim H C, Han C, Kim P, et al. A new measurement method of magnetic flux density using magnetorheological fluid characteristics and a variable resistor circuit[J]. Smart Materials & Structures, 2015, 24(8).

[7] W. Ochoński. Dynamic sealing with magnetic fluids [J]. Wear, 1989, 130(1):261-268.

[8] Mitamura Y, Takahashi S, Amari S, et al. A magnetic fluid seal for rotary blood pumps: Long-term performance in liquid[J]. Physics Procedia, 2010, 9(1):229-233.

[9] Matuszewski L, Szydlo Z. The application of magnetic fluids in sealing nodes designed for operation in difficult conditions and in machines used in sea environment[J]. Polish Maritime Research, 2008,15(3): 49-58.

[10] Li Z. Magnetic fluid seals for DWDM filter manufacturing[J]. Journal of Magnetism & Magnetic Materials, 2002, 252(252):327-329.

[11] Morton G, Früh W G. The force on an object passing through a magnetic fluid seal[J]. Journal of Magnetism & Magnetic Materials, 2002, 252:324-326.

[12] Sun M. A new type zero leaking sealing technology-magnetic fluid sealing[J]. Large Scale Nitrogenous Fertilizer Industry, 2006.

[13] Willenborg K, Kim S, Wittig S. Effects of Reynolds number and pressure ratio on leakage loss and heat transfer in a stepped labyrinth seal[J]. Journal of Turbomachinery, 2001, 123(4):815-822.

[14] Liu T, Cheng Y, Yang Z. Design optimization of seal structure for sealing liquid by magnetic fluids[J]. Journal of Magnetism & Magnetic Materials, 2005, 289:411–414.

[15] Matuszewski L. Multi-stage magnetic-fluid seals for operating in water – life test procedure, test stand and research results[J]. Polish Maritime Research, 2013, 20(1):39-47.

[16] Polevikov V, Tobiska L. Influence of diffusion of magnetic particles on stability of a static magnetic fluid seal under the action of external pressure drop[J]. Communications in Nonlinear Science & Numerical Simulation, 2011, 16(10):4021-4027.

[17] D.C.Li, RP.Xu,X. He, and H.Q.Lan. Study on the magnetic fluid sealing for dry Roots pump. Journal of magnetism and magnetic materials, 2005,289:419-422.

[18] X.L.Yang, Z.L.Zhang, D.C.Li. Numerical and experimental study of agnetic fluid seal with large sealing gap and multiple magnetic sources[J]. Science China Technological Sciences, 2013, 56(11):2865-2869.

[19] Boyson S. Reliability performance of split seal technology when combined with a centrifugal flow device[J].Sealing Technology, 2007, 1(7):7-10.

[20] Belli S, Zhang Y, Pereira P N, et al. Adhesive sealing of the pulp chamber.[J]. Journal of Endodontics, 2001, 27(8):521–526.

[21] Saito C ,, Fusayama T. Adhesive and sealing properties of gallium alloy.[J]. Journal of Dental Research, 1975, 54(4):916-916.

[22] Volkersen O. Die Nietkraftverteilung in zugbeanspruchten nietverbindungen mit konstanten laschenquerschnitten[J]. Luftfahrtforschung 1938, 15(1/2): 41–68.

[23] Adams R.D, Wake W.C. Structural adhesive joints in engineering[R]. 2nd ed. London: Chapman & Hall, 1997.21-25.

[24] Al-Okaily AM, Rogers JA, Ferreira PM. Characterization of delamination in laser micro transfer printing[J]. Micro Nano-Manuf. 2014, 2(1): 1-11.

[25] HUANG Li-ye, XU Ke-wei, LV Jian.Elastic-plastic deformation and fracture mechanism analysis of diamond-like carbon films during nanoscratching[J].Acta metallurgica sinica, 2001, 37(7):733-736

[26] WU Qing-song.The surface roughness application guide[M]. Beijing: China machine press. 1990.7-9. (in Chinese)